(Received 7 March 2025, Accepted 20 May 2025, Scheduled 5 June 2025)

Isosceles Triangle MIMO Antenna for Simultaneous 5G Communications

Mutte Bajibabu[1, 4, *], Jetti Babu[2], and Uppalapati Venkata Ratna Kumari[3]

[1] *Department of Electronics and Communication Engineering, University College of Engineering Jawaharlal Nehru Technological University, Kakinada, Andhra Pradesh, India*
[2] *ECE Department, Dr. Lankapalli Bullayya College of Engineering, Andhra Pradesh, India*
[3] *ECE Department, University College of Engineering Jawaharlal Nehru Technological University, Kakinada, Andhra Pradesh, India*
[4] *ECE Department, Lords Institute of Engineering and Technology, Telangana, India*

ABSTRACT: A four-element compact planar MIMO antenna is developed for the 3.5 GHz 5G sub-6 GHz band, ensuring reliable radiation performance and enabling simultaneous downlink and uplink communication. The proposed MIMO system incorporates four isosceles triangular elements, where two are allocated for uplink and the other two for downlink. Its compact structure facilitates simultaneous communication with separate provisions for uplink and downlink operations. An FR4 substrate has four antennas printed orthogonally to minimize mutual interaction between the elements. Triangles are more isolated and efficient when their corners are trimmed. Cutting the semi-circle yields the desired resonance frequencies. The proposed MIMO system measures $90 \times 90 \times 1.6\,\text{mm}^3$. The performance of the proposed system was evaluated using multiple metrics, including far-field radiation patterns, S-parameters, channel capacity loss, envelope correlation coefficient, peak gain, diversity gain, and radiation efficiency. The simulated results closely aligned with the measured data, demonstrating strong agreement.

1. INTRODUCTION

Due to the restricted spectrum available today, wireless communication technology requires breakthroughs in antenna designs. Small and low-power antennas are necessary for modern wireless devices. Patch antennas are necessary for these applications and are very desirable because of their simple construction. The microstrip line, which has advantages such as being light weight, low profile, simple to manufacture, and basic in structure, feeds these antennas. Patch antennas with a variety of shapes, including circle, ellipse, rectangle, and triangle, were suggested. From them, creating and producing triangles and rectangles is simple [1, 2].

An analysis of the equilateral triangular patch antenna's resonant frequencies is provided [1]. This study presents a small, triangular, triple-band antenna for radio frequency (RF) energy harvesting applications, which allows Internet of Things devices to feed themselves [2]. According to the results, positioning the tuning stub at the triangle's apex is the most efficient way to accomplish circular polarization (CP) radiation [3]. Positioning the tuning stub near the triangle tip is the most efficient way to produce CP radiation [4].

Contemporary wireless communication technologies necessitate high data rates over channels with limited bandwidth. In recent years, there has been growing interest in multiple-input multiple-output (MIMO) systems, which enhance channel capacity by using multiple antennas without additional spectrum or power. A compact MIMO structure is now much more necessary for applications like vehicle-to-vehicle communication, mobile terminal, satellite communication, and base station due to aesthetic and space-saving concerns, which take up more room when being implemented.

Positioning parasitic parts correctly can result in significant improvements in operational BW, isolation, and realized gain. The suggested technique has been used with both multi-element E-coupled and two-element H-coupled MIMO antennas [5]. The primary challenge in MIMO antenna systems is minimizing mutual coupling, which is influenced by the spacing between radiating elements.

The literature has presented a number of methods for reducing mutual coupling. For MIMO systems, a novel microstrip-fed array antenna has been suggested as a workable way to concurrently enhance the array antenna's matching and isolation. These beneficial properties were attained without the need of any traditional matching or isolation framework [6]. Good isolation is achieved using two antenna types on opposite sides of the substrate. Four gap-coupled feed and shorting strips ensure port decoupling and wideband performance.

The radiator sharing technique presented in this study can be adapted to different frequency bands like L, S, C, X, etc. by adjusting the dimensions of the T-shaped ground plate and U-shaped patch [9], and different shape patches can also be used to achieve frequency variation. An irregular patch coupled with inverted-L stubs may generate a resonant point at higher frequencies, while adding an annulus above the main radiator creates a lower resonant point. This approach enables the design of

* Corresponding author: Mutte Bajibabu (bajibabumutte@gmail.com).

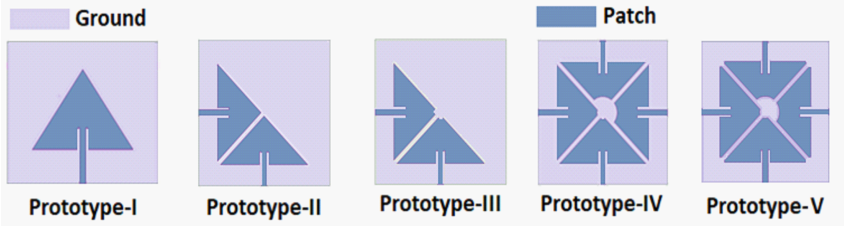

FIGURE 1. Triangle MIMO antenna.

an ultra-low-profile antenna operating within the 3.3–3.6 GHz range [10]. An additional right isosceles triangular microstrip antenna is intended for fundamental mode TM10 [12], while the other is intended for WiMAX applications with a small L-shaped slot [11].

To improve the isolation in dual-band MIMO antennas with closely spaced elements, a decoupling surface and an H-shaped defective ground structure are utilized [13]. Similarly, a compact two-element MIMO antenna for ultra-wideband (UWB) applications, featuring a shared ground plane, incorporates an electromagnetic band gap (EBG) structure positioned as a single column between two rectangular patches, along with a ground plane stub [14, 15]. Furthermore, the use of terminated coupled lines in wide stopband filtering patch antennas and their integration into MIMO array systems are investigated in [16].

These models use guard band, guard period, and discontinuous transmission to offer isolation for both uplink and downlink communications. Base stations must be synchronized to reduce crosslink interference [17]. FSS structure is used to increase the gain and decrease the antenna size [23] which results in enhancement in antenna performance. Multi-narrowband technology is essential for enabling simultaneous uplink and downlink communications, effectively mitigating challenges like discontinuous transmission and interference. Studies have reportedly used two independent U-slot rectangular microstrips to provide simultaneous communications. Base station U and π slot triple band uplink and downlink antennas are designed [19, 20].

Miniaturized multi-narrow band MIMO is therefore observed to be essential for providing simultaneous communications along with excellent isolation among the individual elements. A four-triangle MIMO antenna arrangement is suggested in this paper for simultaneous communications. A comprehensive overview of the proposed antenna's design, construction, feeding arrangement, and diversity performance is presented, with results analysed through both simulations and measurements.

2. ANTENNA DESIGN AND STRUCTURAL CONFIGURATION

2.1. Antenna Structure Evolution

Figure 1 displays the geometry of the Isosceles Triangle MIMO antenna. The proposed structure is divided into different quadrants, and by rotating first the design is evolved. Initially, Isosceles Triangle antenna is designed and constructed on FR4 ($\epsilon_r = 4.4$) with a substrate height (h) of 1.6 mm [11]. The resonant frequency is tuned by adjusting the triangle's side lengths, while the inset feed line's dimensions ensure impedance matching. A finite ground plane prevents bidirectional radiation.

An inset fed triangular patch antenna was first created, with the inset feed matching the impedance and was shown in the first prototype. Prototype II displays another triangular inset feeding antenna that is positioned orthogonally to fulfil MIMO requirements. Prototype III illustrates how to shorten the corner length with radius "a" or "b" from the centre — exactly the centre of the substrate to obtain the required frequency. Prototype IV illustrates how two more identical triangle antennas are positioned orthogonally to the first two in order to enable simultaneous communication. Prototype V illustrates how reducing the corners of each part lowers the mutual coupling. Figure 2 displays the changes in resonance frequency of the prototypes.

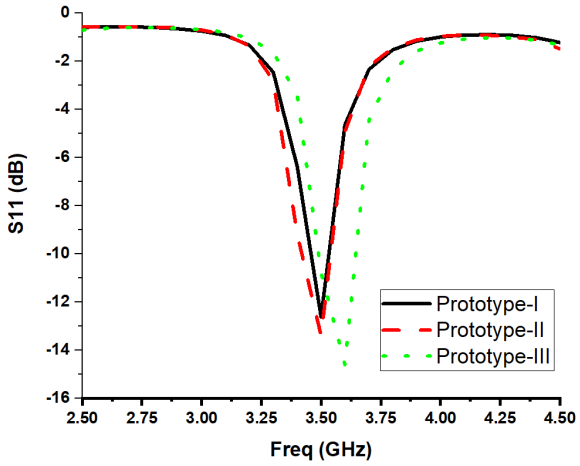

FIGURE 2. Return loss of Triangle MIMO antenna.

2.2. Design Expressions

$$\mathbf{f_r} = \frac{\mathbf{P_{mn}v}}{\mathbf{2\pi\sqrt{\varepsilon_r}}} \tag{1}$$

where,

$$\mathbf{P_{mn}} = \frac{\mathbf{\sqrt{2}m\pi}}{\mathbf{\frac{K}{2}-\left(\frac{a+c}{2}\right)}} \text{ for uplink} \tag{2}$$

$$\mathbf{P_{mn}} = \frac{\mathbf{\sqrt{2}m\pi}}{\mathbf{\frac{K}{2}-\left(\frac{b+c}{2}\right)}} \text{ for downlink} \tag{3}$$

$$\mathbf{v} = \textbf{Velocity}$$

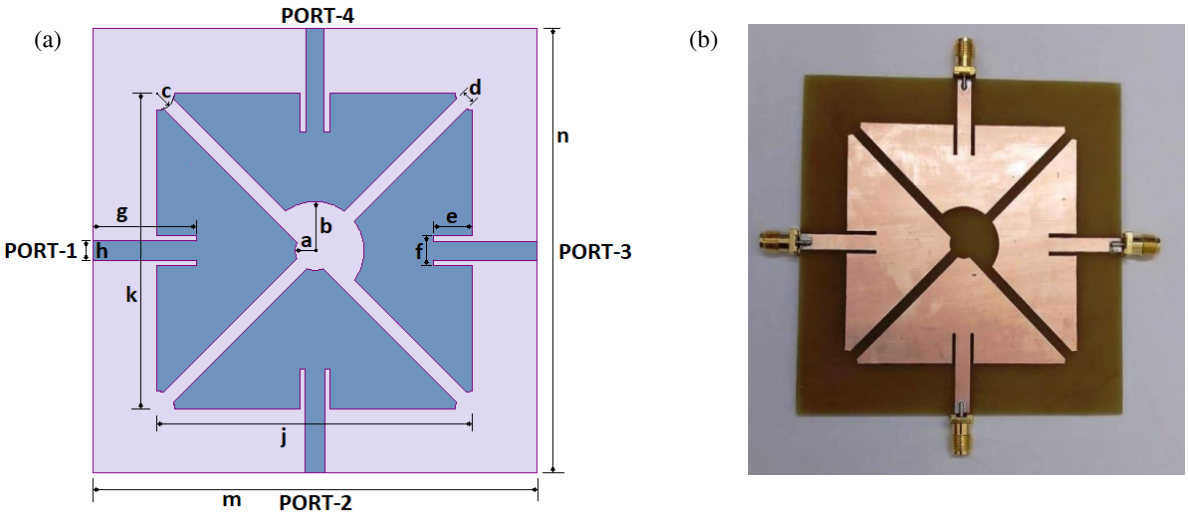

FIGURE 3. Triangle MIMO antenna. (a) Geometry (b) Fabricated antenna. Dimensions (in mm): $a = 4$ mm, $b = 8$ mm, $c = 3.5$ mm, $d = 2$ mm, $e = 8$ mm, $f = 6$ mm, $g = 21$ mm, $h(uplink) = 4$ mm, $h(downlink) = 3.8$ mm, $j = 64$ mm, $k = 64$ mm, $m = 90$ mm, $n = 90$ mm.

The above design expressions were used in the design process of MIMO elements [11].

2.3. MIMO Geometry

It is necessary to construct the downlink and uplink independently to satisfy the need for simultaneous communications. The appropriate side lengths of the triangles and the parameters 'a' or 'b' are carefully considered in the design to achieve the desired uplink and downlink communication frequencies. As seen in Figure 3, the suggested MIMO antenna consists of four triangle antennas, two of which are used for uplink and two more for downlink. For the downlink of the MIMO antennas, ports P3 and P4 are chosen as they are beside each other, while ports P1 and P2 are selected for uplink MIMO antennas. The proposed antenna, designed on an FR4 dielectric substrate with dimensions of 90×90 mm and a thickness of 1.6 mm, is modelled and thoroughly analysed using High Frequency Structure Simulator (HFSS) software for simulation.

Finally, the positions of the uplink antennas' ports P1 and P2 are diagonal, as seen in Figure 3. In the same manner, downlink antenna ports P3 and P4 are positioned. In addition, note that ports P2, P4 & P1, P3 are orthogonal to one another. Reducing the mutual coupling between pieces by patch-cutting enhances diversity performance as well. In Figures 3(a) and (b), the designed and manufactured 4-port antenna with trianle-shaped MIMO antenna geometry is presented. The compact and planar structure of the proposed MIMO antenna makes it simple to integrate into real-world systems for pertinent applications.

3. RESULTS AND DISCUSSION

3.1. Triangle Uplink MIMO Antenna

The sub-6 5G frequency is where the isosceles triangle uplink antenna is intended to function. The frequency range for 5G uplink and downlink communications is 3300–3800 MHz. The measured and predicted return losses were -26 dB at 3.55 GHz and -22.9 dB at 3.5 GHz, respectively. By activating port P1 and closing all other ports, one may determine the uplink return loss. Figure 4 shows the observed impedance bandwidth for the same 3520–3650 MHz as well as the simulated impedance bandwidth of 3440–3610 MHz. In the designated spectrum, a bandwidth of more than 130 MHz is attained.

Figure 5 illustrates the measured and simulated radiation patterns of the uplink antenna at 3.5 GHz. The radiation patterns were recorded in the far-field region, with a horn antenna for transmission and the proposed antenna for reception. Measurements were conducted with port P1 active, while all other ports were terminated with matching loads. The measured peak gain in the E plane was 2.19 dB, and simulated one was 2.31 dB. The measured and simulated total gain patterns are plotted for $\Phi = 0°$ and $\Phi = 90°$. Within the H-plane, the measured peak gain in the E-plane was 2.05 dB, and simulated one was 2.3 dB.

Comparably, simulation yields an efficiency of 54.62% whereas measured findings show 52.45%. In both outcomes, cross polarizations are 19 dBi. Table 1 is a list of the peak gains.

3.2. Triangle Multi-Band Downlink Antenna

The sub-6 5G frequency is where the isosceles triangle downlink antenna is intended to function. The frequency range for 5G uplink and downlink communications is 3300–3800 MHz. Feeding input to port P3 and terminating all other ports gives the return loss of the downlink. The measured and predicted return losses were -21 dB at 3.75 GHz and -19.6 dB at 3.7 GHz, respectively. Figure 4 shows the measured impedance bandwidth for the same frequency range of 3730–3810 MHz, which differs from the simulated impedance bandwidth of 3660–3770 MHz. A bandwidth of greater than 80 MHz is attained in the specified band.

In Figure 6, the simulated and measured polar radiation patterns of the downlink antenna are at a frequency of 3.75 GHz. The total gain patterns, both simulated and measured, are plot-

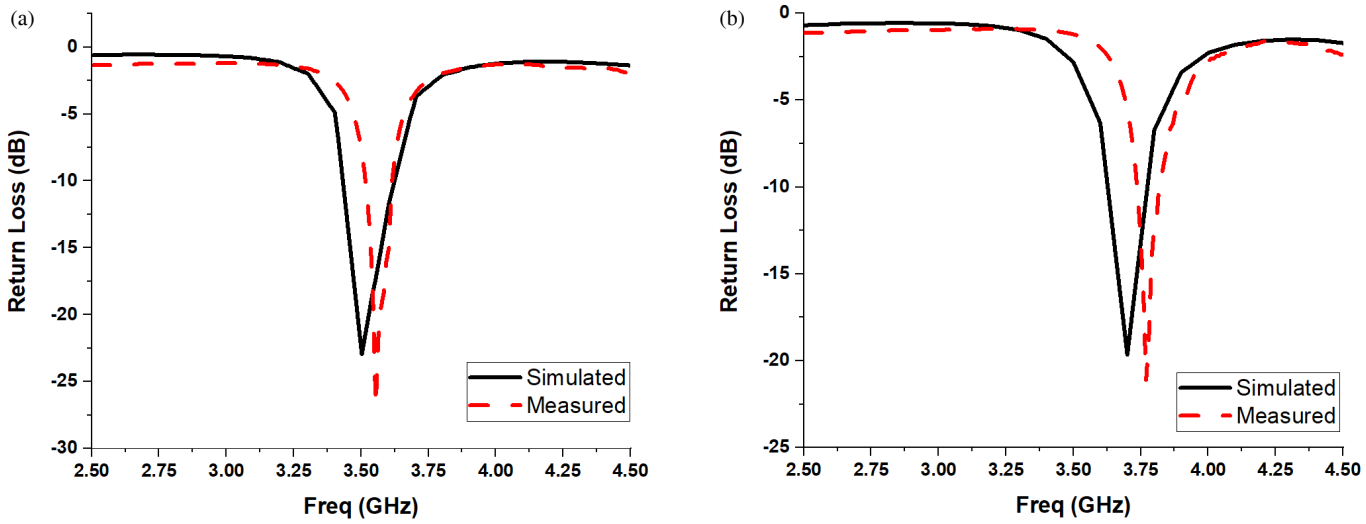

FIGURE 4. The isosceles triangle, (a) uplink MIMO antenna's return loss and (b) downlink MIMO antenna's return loss.

TABLE 1. Comparison of the suggested antenna with the MIMO antennas currently in use.

Ref.	Size (mm) ($L \times W \times H$)	Freq. (GHz)	Band Width (MHz)	Isolation (dB)	ECC	Gain (dBi)
[6]	$40 \times 32 \times 1$	f_1: 5.5	BW_1: 290	> 30	< 0.15	f_1: 4.79
[7]	$80 \times 60 \times 2.6$	f_1: 2.4	BW_1: 900	> 20	< 0.02	f_1: 2.3
[9]	$75 \times 59 \times 19$	f_1: 3.7 f_2: 4.1	BW_1: 40 BW_2: 35	> 25	< 0.01	f_1: 8.5 f_2: 7.9
[10]	$120 \times 24 \times 1.6$	f_1: 4.1 f_2: 4.9	BW_1: 600 BW_2: 290	> 18	< 0.25	f_1: 5.01 f_2: 5.38
[18]	$70 \times 130 \times 1.6$	f_{1U}: 0.902 f_{2U}: 1.68 f_{3U}: 2.535	BW_1: 27 BW_2: 31 BW_3: 53	> 25	< 0.12	f_{1U}: 1.62 f_{2U}: 1.94 f_{3U}: 1.87
		f_{1D}: 0.939 f_{2D}: 1.869 f_{3D}: 2.547	BW_1: 13 BW_2: 33 BW_3: 45			f_{1D}: 2.36 f_{2D}: 3.13 f_{3D}: 2.84
PROPOSED	$90 \times 90 \times 1.6$	f_{1U}: 3.55	BW_1: 50	> 19	< 0.1	f_{1U}: 2.31
		f_{1D}: 3.75	BW_1: 45			f_{1D}: 2.61

Frequency of resonance (f), Band width (BW), not given (NG), D: Downlink and U: Uplink

ted at $\Phi = 0°$ and $\Phi = 90°$. In the E-plane, the peak gain achieved was 2.61 dB in simulation and 2.39 dB in measurements, while in both the H-plane and E-plane, it was 2.6 dB in simulation and 2.52 dB in measurements.

In both cases, cross polarizations were 18 dBi. Table 1 is a list of the peak gains.

Port 1 of the uplink antenna is stimulated, and every other port is terminated with a matching load. Figure 7 displays the distribution of surface current. In Subsection 3.1, this is explained in depth using three alternative examples. The current distribution is observed to be identical to the downlink antenna depicted in Figure 7 when port-4 is excited in the downlink antenna, and all other ports are terminated with matching loads.

Table 1 shows the comparison of the proposed antenna with the existing MIMO antennas.

3.3. Isolation between MIMO Antenna

Mutual coupling, critical in MIMO systems with a required minimum of 12 dB isolation between ports, is minimized by orthogonally arranging the uplink and downlink antenna elements, with the downlink elements positioned diagonally to further enhance isolation and improve system efficiency. In addition, note that ports P2, P4 & P1, P3 are orthogonal to one another. Reducing the mutual coupling between pieces by patch-cutting enhances diversity performance as well.

In the simulation, a separation exceeding 26 dB was achieved between the downlink elements (P3 and P4) and the uplink elements (P1 and P2). Additionally, simulated isolation levels above 23 dB were observed between the uplink and downlink pairs as illustrated in Figure 8. By removing corners copper in the patch, it is observed that the isolation increases by 3 dB.

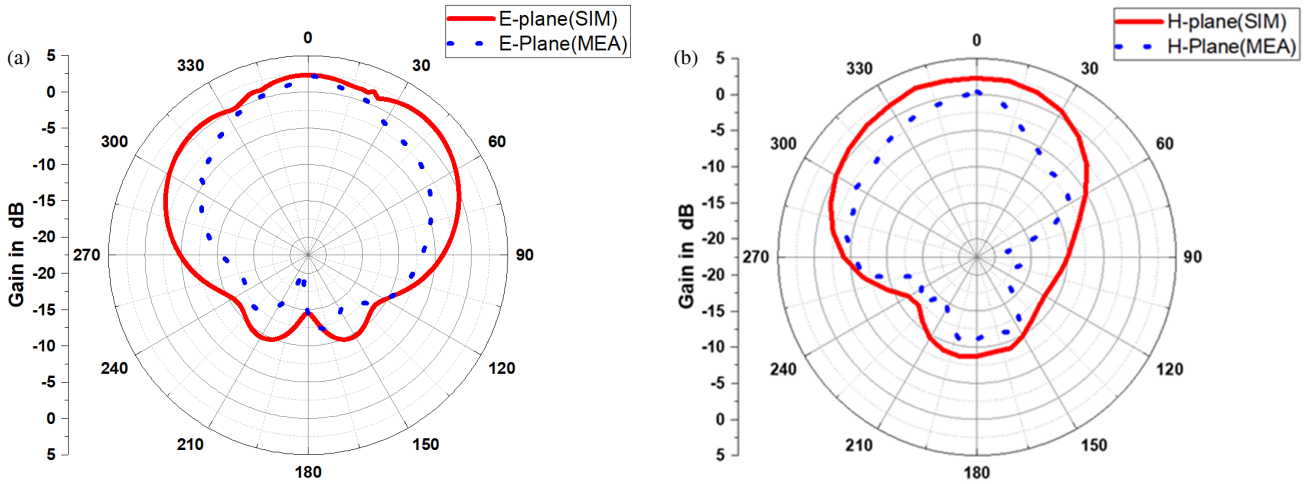

FIGURE 5. Radiation patterns of uplink antenna. (a) E-Plane, (b) H-Plane.

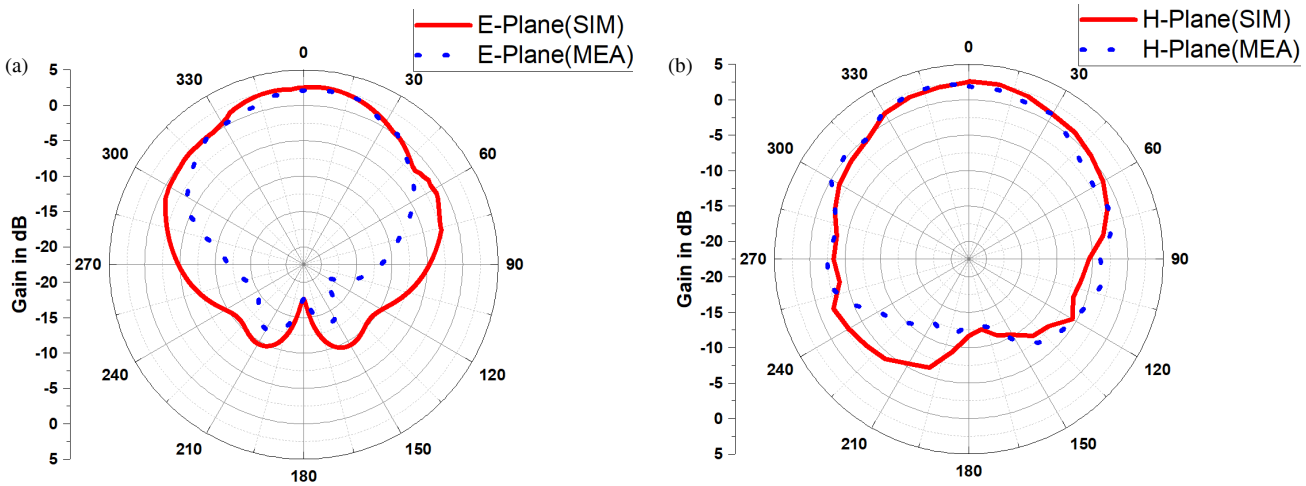

FIGURE 6. Radiation patterns of downlink antenna. (a) E-plane, (b) H-plane.

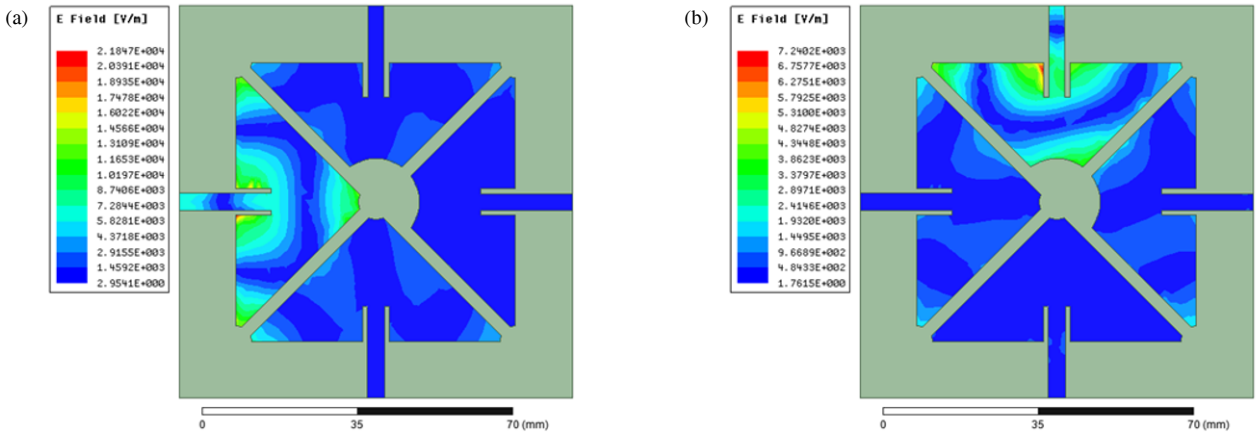

FIGURE 7. Current distribution of (a) uplink antenna (b) downlink antenna.

4. DIVERSITY PERFORMANCE OF MIMO ANTENNAS

Envelope correlation coefficient (ECC) is a key metric for assessing the diversity performance of a MIMO system. ECC and diversity gain are measured respectively for both uplink and downlink MIMO antennas. ECC can be calculated using two different methods. Using recorded far-field radiation patterns and a mathematical calculation using the formula below, the first method yields ECC (ρ_e) [21].

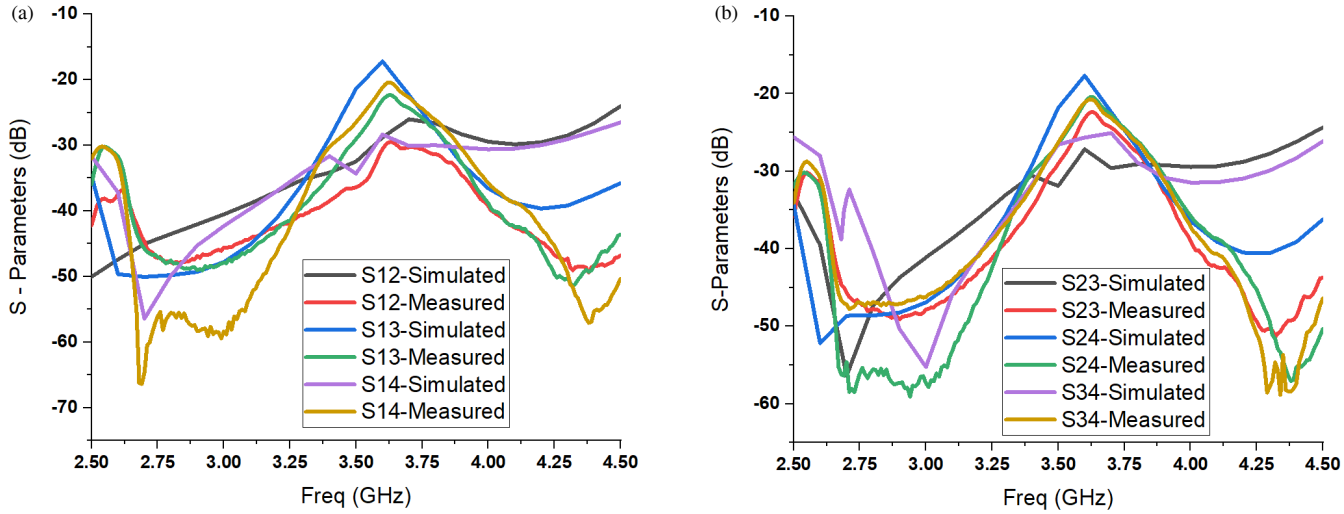

FIGURE 8. Mutual coupling between the MIMO antenna elements (a) S12, S13 and S14 (b) S23, S24 and S34.

$$\mathbf{ECC}(\boldsymbol{\rho}_{\mathbf{e}}) = \frac{\left| \oiint_{\Omega} \left[\mathbf{E_i}\left(\boldsymbol{\theta}, \boldsymbol{\Phi}\right) \cdot \mathbf{E_j}\left(\boldsymbol{\theta}, \boldsymbol{\Phi}\right) \right] \mathbf{d\Omega} \right|^2}{\oiint_{\Omega} \left[\left|\mathbf{E_{\theta i}}\left(\boldsymbol{\theta}, \boldsymbol{\Phi}\right)\right|^2 + \left|\mathbf{E_{\Phi i}}\left(\boldsymbol{\theta}, \boldsymbol{\Phi}\right)\right|^2 \right] \mathbf{d\Omega} \oiint_{\Omega} \left[\left|\mathbf{E_{\theta j}}\left(\boldsymbol{\theta}, \boldsymbol{\Phi}\right)\right|^2 + \left|\mathbf{E_{\Phi j}}\left(\boldsymbol{\theta}, \boldsymbol{\Phi}\right)\right|^2 \right] \mathbf{d\Omega}} \tag{4}$$

where,

$$E_i(\theta, \Phi) \cdot E_j(\theta, \Phi) = E_{\theta i}(\theta, \Phi) E^*_{\theta j}(\theta, \Phi) + E_{\Phi i}(\theta, \Phi) E^*_{\Phi j}(\theta, \Phi) \tag{5}$$

E_θ and E_Φ are the electric field components and patterns of elevation angle (θ) and azimuth angle (Φ), respectively. Here, i and j refer to P1 and P2, respectively, for an uplink MIMO antenna. In the case of the downlink MIMO antenna, i and j stand for P3 and P4, respectively. Calculating the downlink MIMO antenna's electric field components involves stimulating port P1 and terminating the other ports with a matching load. All other ports' components of the electric field are obtained in a similar fashion, which involves activating each port in turn and terminating the others. For both downlink and uplink MIMO antennas, the diversity gain exceeds 9.88 dBi, and the ECC values are less than 0.1.

The second method uses S-parameters to obtain the ECCs of both uplink and downlink MIMO antennas [21]. The following formulas can be used to compute the ECC and diversity gain of uplink and downlink antennas.

$$\mathbf{ECC}(\rho_{\mathbf{eu}}) = \frac{\left|\mathbf{S_{11}^*}\,\mathbf{S_{12}} + \mathbf{S_{21}^*}\,\mathbf{S_{22}}\right|^2}{\left(\mathbf{1} - \left|\mathbf{S_{11}}\right|^2 - \left|\mathbf{S_{21}}\right|^2\right)\left(\mathbf{1} - \left|\mathbf{S_{22}}\right|^2 - \left|\mathbf{S_{12}}\right|^2\right)} \tag{6}$$

$$\mathbf{ECC}(\rho_{\mathbf{ed}}) = \frac{\left|\mathbf{S_{33}^*}\,\mathbf{S_{34}} + \mathbf{S_{43}^*}\,\mathbf{S_{44}}\right|^2}{\left(\mathbf{1} - \left|\mathbf{S_{33}}\right|^2 - \left|\mathbf{S_{43}}\right|^2\right)\left(\mathbf{1} - \left|\mathbf{S_{44}}\right|^2 - \left|\mathbf{S_{34}}\right|^2\right)} \tag{7}$$

$$\text{Diversity Gain (Uplink)} = 10\sqrt{1 - \left|\mathrm{ECC}(\boldsymbol{\rho}_{\mathrm{eu}})\right|^2} \tag{8}$$

$$\text{Diversity Gain (Downlink)} = 10\sqrt{1 - \left|\mathrm{ECC}(\boldsymbol{\rho}_{\mathrm{ed}})\right|^2} \tag{9}$$

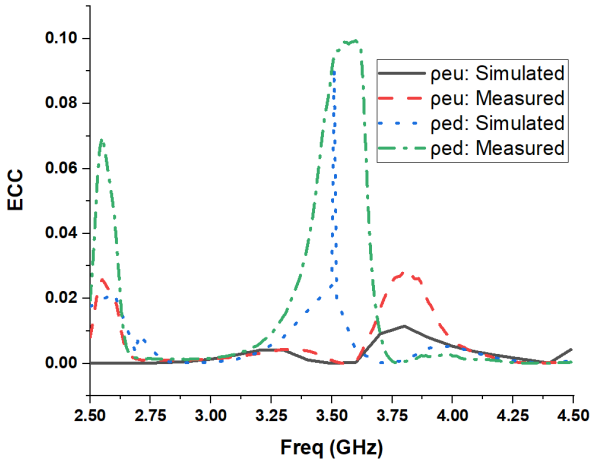

FIGURE 9. ECC of triangle MIMO antenna.

Figure 9 shows the diversity gain surpassing 9.9 dBi and ECC values below 0.1 for all the downlink and uplink MIMO antennas. Both ECC and diversity gain calculations are found within an acceptable range using both methods [22].

5. CONCLUSION

This study presents an arrangement of four isosceles triangle MIMO antennas and discusses its uses for both uplink and downlink communications in sub-6 base stations. In the designated band, a return loss of less than −19 dB is attained. Practically speaking, an uplink antenna's impedance bandwidth is 130 MHz, while downlink antenna's impedance bandwidth is 80 MHz. Additionally, the experimental findings demonstrate

that the suggested antenna in the designated bands achieved 54% efficiency, 19 dBi cross polarisations, and a peak gain of over 2.05 dBi. Practical research yields an isolation of greater than 23 dB, which enhances the MIMO system's diversity performance. In the designated frequency band, the computed ECC values are below 0.1, indicating excellent performance. The proposed MIMO antenna, with its compact and flat design, is easy to integrate into practical systems. Furthermore, the measured results align well with the simulation data, demonstrating the effectiveness of the design.

REFERENCES

[1] Chen, W., K.-F. Lee, and J. S. Dahele, "Theoretical and experimental studies of the resonant frequencies of the equilateral triangular microstrip antenna," *IEEE Transactions on Antennas and Propagation*, Vol. 40, No. 10, 1253–1256, Oct. 1992.

[2] Benkalfate, C., A. Ouslimani, A.-E. Kasbari, and M. Feham, "A new compact triple-band triangular patch antenna for RF energy harvesting applications in IoT devices," *Sensors*, Vol. 22, No. 20, 8009, 2022.

[3] Lu, J.-H. and K.-L. Wong, "Single-feed circularly polarized equilateral-triangular microstrip antenna with a tuning stub," *IEEE Transactions on Antennas and Propagation*, Vol. 48, No. 12, 1869–1872, Dec. 2000.

[4] Chen, J., C. Jin, B. Zhang, and Z. Shen, "Combined triangle quarter-wavelength patches and their application to high-gain CP antenna," *IEEE Antennas and Wireless Propagation Letters*, Vol. 19, No. 1, 104–108, Jan. 2020.

[5] Tran, H. H. and N. Nguyen-Trong, "Performance enhancement of MIMO patch antenna using parasitic elements," *IEEE Access*, Vol. 9, 30 011–30 016, 2021.

[6] Ghannad, A. A., M. Khalily, P. Xiao, R. Tafazolli, and A. A. Kishk, "Enhanced matching and vialess decoupling of nearby patch antennas for MIMO system," *IEEE Antennas and Wireless Propagation Letters*, Vol. 18, No. 6, 1066–1070, Jun. 2019.

[7] Li, H., J. Xiong, and S. He, "A compact planar MIMO antenna system of four elements with similar radiation characteristics and isolation structure," *IEEE Antennas and Wireless Propagation Letters*, Vol. 8, 1107–1110, 2009.

[8] Wong, K.-L., J.-Z. Chen, and W.-Y. Li, "Four-port wideband annular-ring patch antenna generating four decoupled waves for 5G multi-input-multi-output access points," *IEEE Transactions on Antennas and Propagation*, Vol. 69, No. 5, 2946–2951, May 2021.

[9] Niu, Z., H. Zhang, Q. Chen, and T. Zhong, "Isolation enhancement in closely coupled dual-band MIMO patch antennas," *IEEE Antennas and Wireless Propagation Letters*, Vol. 18, No. 8, 1686–1690, Aug. 2019.

[10] Zhou, J. and M. Yang, "Design of six port antenna with frequency diversity and diverse radiation pattern," *IEEE Access*, Vol. 10, 65 962–65 970, 2022.

[11] Sharma, V., S. Shekhawat, V. K. Saxena, J. S. Saini, K. B. Sharma, B. Soni, and D. Bhatnagar, "Right isosceles triangular microstrip antenna with narrow L-shaped slot," *Microwave and Optical Technology Letters*, Vol. 51, No. 12, 3006–3010, 2009.

[12] Maity, S. and B. Gupta, "Approximate investigation on isosceles triangular microstrip antenna in fundamental mode," *Microwave and Optical Technology Letters*, Vol. 59, No. 3, 614–618, 2017.

[13] Zhai, H., J. Zhang, Y. Zang, Q. Gao, and C. Liang, "An LTE base-station magnetoelectric dipole antenna with anti-interference characteristics and its MIMO system application," *IEEE Antennas and Wireless Propagation Letters*, Vol. 14, 906–909, 2014.

[14] Iqbal, A., O. A. Saraereh, A. W. Ahmad, and S. Bashir, "Mutual coupling reduction using F-shaped stubs in UWB-MIMO antenna," *IEEE Access*, Vol. 6, 2755–2759, 2017.

[15] Khan, A., S. Bashir, S. Ghafoor, and K. K. Qureshi, "Mutual coupling reduction using ground stub and EBG in a compact wideband MIMO-antenna," *IEEE Access*, Vol. 9, 40 972–40 979, 2021.

[16] Qian, J.-F., F.-C. Chen, Y.-H. Ding, H.-T. Hu, and Q.-X. Chu, "A wide stopband filtering patch antenna and its application in MIMO system," *IEEE Transactions on Antennas and Propagation*, Vol. 67, No. 1, 654–658, Jan. 2019.

[17] Holma, H. and A. Toskala, *LTE for UMTS: OFDMA and SC-FDMA Based Radio Access*, John Wiley & Sons, 2009.

[18] Huang, H., X. Li, and Y. Liu, "A low-profile, dual-polarized patch antenna for 5G MIMO application," *IEEE Transactions on Antennas and Propagation*, Vol. 67, No. 2, 1275–1279, Feb. 2019.

[19] Goud, J. R., N. V. K. Rao, and A. M. Prasad, "Design of triple band U-slot MIMO antenna for simultaneous uplink and downlink communications," *Progress In Electromagnetics Research C*, Vol. 106, 271–283, 2020.

[20] Jangampally, R. G., V. K. R. Nalam, and M. P. Avala, "Design of uplink and downlink triple band π: Slot antennas for simultaneous communication," *Wireless Personal Communications*, Vol. 124, No. 4, 3189–3203, 2022.

[21] Blanch, S., J. Romeu, and I. Corbella, "Exact representation of antenna system diversity performance from input parameter description," *Electronics Letters*, Vol. 39, No. 9, 705–707, 2003.

[22] Zhai, H., L. Xi, Y. Zang, and L. Li, "A low-profile dual-polarized high-isolation MIMO antenna arrays for wideband base-station applications," *IEEE Transactions on Antennas and Propagation*, Vol. 66, No. 1, 191–202, Jan. 2018.

[23] Solunke, Y. and A. Kothari, "An ultra-thin, low-RCS, dual-bandpass novel fractal-FSS for planar/conformal C&X bands applications," *AEU — International Journal of Electronics and Communications*, Vol. 175, 155073, 2024.

[24] Sanugomula, M. and K. K. Naik, "A compact high gain circular shaped two-port MIMO antenna with fractal DGS for downlink satellite communication," *Progress In Electromagnetics Research M*, Vol. 125, 135–142, 2024.